

## L1157-B1: Water and ammonia as diagnostics of shock temperature

Viti S. <sup>1</sup>, Jimènez-Serra, I <sup>2</sup>, Yates J. A. <sup>1</sup>, Codella C. <sup>3</sup>, Vasta M. <sup>3</sup>, Caselli P. <sup>4,3</sup> Lefloch B. <sup>5,6</sup> Ceccarelli C. <sup>5</sup>

sv@star.ucl.ac.uk

Received \_\_\_\_\_; accepted \_\_\_\_\_

---

<sup>1</sup>Department of Physics and Astronomy, University College London, Gower Street, London, WC1E 6BT, UK

<sup>2</sup>Harvard-Smithsonian Center for Astrophysics, 60 Garden Street, Cambridge, MA 02138, USA

<sup>3</sup>INAF, Osservatorio Astrofisico di Arcetri, Largo E. Fermi 5, 50125, Firenze, Italy

<sup>4</sup>School of Physics and Astronomy, University of Leeds, Leeds, LS2 9JT, UK

<sup>5</sup>UJF-Grenoble 1/CNRS-INSU, Institut de Plantologie et d'Astrophysique de Grenoble (IPAG) UMR 5274, Grenoble, France

<sup>6</sup>Centro de Astrobiologia, CSIC-INTA, Carretera de Ajalvir, Km 4, Torrejon de Ardoz, 28850, Madrid, Spain

## ABSTRACT

We investigate the origin and nature of the profiles of water and ammonia observed toward the L1157-B1 clump as part of the HIFI CHESS survey (Ceccarelli et al. 2010) using a new code coupling a gas-grain chemical model with a parametric shock model. First results from the unbiased survey (Lefloch et al. 2010, Codella et al. 2010) reveal different molecular components at different excitation conditions coexisting in the B1 bow shock structure, with  $\text{NH}_3$ ,  $\text{H}_2\text{CO}$  and  $\text{CH}_3\text{OH}$  emitting only at relatively low outflow velocities whereas  $\text{H}_2\text{O}$  shows bright emission at high velocities. Our model suggests that these differences are purely chemical and can be explained by the presence of a C-type shock whose maximum temperature must be close to 4000 K along the B1 clump.

*Subject headings:* ISM: individual objects: L1157 — ISM: molecules — stars: formation

## 1. Introduction

During the earliest stage of star formation, protostars generate fast jets. The supersonic impact between the jet and the parent cloud generates shock fronts propagating through the high-density gas surrounding the protostar. The shocks heat and compress the ambient gas, and complex chemistry driven by endothermic chemical reactions, ice grain mantle sublimation and sputtering occur. Several molecules, such as  $\text{H}_2\text{O}$ ,  $\text{NH}_3$ ,  $\text{CH}_3\text{OH}$ ,  $\text{H}_2\text{CO}$ , undergo abundance enhancements by orders of magnitude (e.g. Draine et al. 1983; Kaufman & Neufeld, 1996), as observed at mm-wavelengths in a number of outflows (Garay et al. 1998; Bachiller & Pérez Gutiérrez 1997; Jiménez-Serra et al. 2005; Jørgensen et al. 2007).

One of the best laboratories is the L1157 region located at a distance between 250 and 440 pc, where a Class 0 protostar (L1157-mm) drives a chemically rich bipolar outflow (e.g. Gueth et al. 1996, Bachiller et al. 2001). The outflow is associated with several bow shocks seen in IR  $\text{H}_2$  (Nisini et al. 2010), in CO (Gueth et al. 1996) as well as in other molecules (Bachiller & Pérez Gutiérrez 1997) thought to be released from icy mantles such as  $\text{H}_2\text{CO}$ ,  $\text{CH}_3\text{OH}$ , and typical tracers of high-speed shocks such as SiO, sputtered from dust grains (Caselli et al. 1997; Gusdorf et al. 2008; Jiménez-Serra et al. 2008). The brightest bow-shock, L1157-B1, has been extensively studied from the ground using IRAM-PdB and NRAO-VLA interferometers, revealing a rich and clumpy structure (Tafalla & Bachiller 1995; Benedettini et al. 2007; Codella et al. 2009).

As part of the Herschel Key Program CHES (Chemical Herschel Surveys of Star forming regions, Ceccarelli et al. 2010), L1157-B1 has been investigated with a spectral survey in the  $\sim 500\text{--}2000$  GHz interval using the HIFI instrument to provide high-resolution (1 MHz) spectra. Preliminary results (Codella et al. 2010; Lefloch et al. 2010) have not only confirmed the chemical richness of the L1157-mm outflow, but have also revealed the presence of different molecular components at different excitation conditions coexisting in

the B1 structure. In addition, the CHESS data have allowed, for the first time, comparison of the line profiles of tracers of shocked material such as  $\text{CH}_3\text{OH}$ ,  $\text{H}_2\text{CO}$ , with those due to the fundamental transitions of water and ammonia. These species show two different kinds of profiles, with  $\text{CH}_3\text{OH}$ ,  $\text{H}_2\text{CO}$ , and  $\text{NH}_3$  emitting only at relatively low outflow velocities ( $\sim 15 \text{ km s}^{-1}$  with respect to the ambient velocity), whereas  $\text{H}_2\text{O}$  shows bright emission even at the highest velocities (up to  $30 \text{ km s}^{-1}$ ), as seen in  $\text{SiO}$  (e.g. Zhang et al. 1995) and  $\text{CO}$  (Lefloch et al. 2010). The intensity of methanol, formaldehyde, and ammonia with respect to  $\text{H}_2\text{O}$  decreases towards higher outflow velocities suggesting, in case of optically thin emission, a similar decrease in the abundance ratios. Note that while  $\text{SiO}$  and  $\text{CO}$  are not products of surface reactions,  $\text{H}_2\text{O}$ ,  $\text{NH}_3$ ,  $\text{CH}_3\text{OH}$  and  $\text{H}_2\text{CO}$  are all highly enhanced on the dust grains, and therefore the distinct behaviour of water is worth investigating.

High  $\text{NH}_3$  abundances in the gas phase have been observed in many warm regions (e.g. hot cores and outflows, Beuther et al. 2005; Sepulveda et al. 2011).  $\text{NH}_3$  is believed to be mainly a direct product of grain surface reactions (although at high temperatures ammonia can also form in gas phase, reaching abundances of  $\sim 10^{-5}$  - see Section 3) with nitrogen hydrogenating until saturation as it sticks to the dust during the cold phase (e.g. Brown et al. 1988; Viti et al. 2004a). Water is enhanced by the release of the icy mantles *as well as* by endothermic reactions occurring in the warm ( $\geq 220 \text{ K}$ ) shocked gas, which convert the bulk of atomic oxygen into water (e.g. Kaufman & Neufeld 1996, and references therein).

In this Letter we investigate the differences between the water and ammonia profiles by using a new code which couples a gas-grain chemical model with a parametric shock model.

## 2. The model

The gas-grain chemical code UCL\_CHEM (Viti et al. 2004a) was coupled with the parametric shock model developed by Jiménez-Serra et al. (2008). UCL\_CHEM is a time dependent gas-grain chemical model in two phases. During Phase I, gravitational collapse, gas-phase chemistry and sticking on to dust particles with subsequent processing occur. This phase simulates the formation of high density clumps and starts from a diffuse ( $\sim 100 \text{ cm}^{-3}$ ) medium in atomic form (apart from a fraction of hydrogen in  $\text{H}_2$ ). The initial abundances adopted are solar but different initial values for the sulfur elemental abundance were also used. Atoms and molecules are depleted onto grain surfaces as in Rawlings et al. (1992, Eq. 2) and hydrogenate when possible. The depletion efficiency is determined by the fraction of the gas-phase material that is frozen onto the grains. This approach allows a derivation of the ice composition. Phase II computes the time dependent chemical evolution of the gas and dust once the clump has formed and stellar activity is present (in the form of a protostar and/or outflows). Full details of the code can be found in Viti et al. (2004a). For this work the UCL\_CHEM was coupled with the parametric shock model of Jiménez-Serra et al. (2008) which calculates the physical structure of a plane-parallel steady-state C-shock that propagates with a velocity  $v_s$  through an unperturbed medium. This approximation was validated by comparing its results with those from magnetohydrodynamic (MHD) C-shock modelling (Flower et al. 2003, Kaufman & Neufeld 1996). Although not strictly accurate, the general behaviour of the velocity of the ion and neutral fluids (i.e.  $v_i$  and  $v_n$ ), of the density of the neutral particles ( $n_n$ ), and of the temperature of the ions and neutrals ( $T_i$  and  $T_n$ ), mimics the MHD physical structure of C-shocks (Figures 1 and 2 in Jiménez-Serra et al. 2008).

In addition to the C-shock physical structure, the parametric model includes the sputtering of dust grains following the formalism used by Caselli et al. (1997), updated with

the results from May et al. (2000). In our chemical model, the icy mantles are sputtered once the dynamical age across the C-shock has reached the ‘saturation time-scales’ (or  $t_{sat}$ ; Jiménez-Serra et al. 2008). These are the time-scales for which almost all molecular material within the mantles is released into the gas. In Jiménez-Serra et al. (2008),  $t_{sat}$  were originally derived for SiO (see their Table 5). However, we adopt the same  $t_{sat}$  values for H<sub>2</sub>O and NH<sub>3</sub> because the mathematical expressions of the fraction of SiO, H<sub>2</sub>O and NH<sub>3</sub> sputtered from the grain mantles are the same for all these molecular species except for their initial abundance contained in the mantles (see Appendix B in Jiménez-Serra et al. 2008). The adopted  $t_{sat}$  for H<sub>2</sub>O and NH<sub>3</sub> were finally scaled for the different initial H<sub>2</sub> densities explored in our study, by assuming <sup>1</sup> that  $t_{sat} \propto n_n^{-1}$ .

For this work, Phase I was used to form the pre-existing (to the shock) clump, B1. We do not know how dense the pre-existing clump was; however modelling of the clumps along a similar outflow (CB3; Viti et al. 2004b; Benedettini et al. 2006) has shown that in order for the chemistry to be as rich as observed, some level of clumpiness must pre-exist the shock; hence we did not consider final densities for Phase I lower than 1000 cm<sup>-3</sup> (see Table 1). The shock model was then included in the Phase II of the chemical model.

A total of 15 models were run (Table 1) where we varied: i) the final densities of Phase I (and hence the initial density of the clump before it became shocked); we have restricted these densities to the range between 10<sup>3</sup> to 10<sup>5</sup> cm<sup>-3</sup>, similar to those derived by Güsdorf et al. (2008) and Nisini et al. (2010) for the B1 clump. Higher pre-shock densities have not been considered in this study because the collisional dissociation of H<sub>2</sub> would highly overcome the formation rate of H<sub>2</sub>, leading to the development of a J-type discontinuity within the physical structure of the shock for the shock velocities we are considering (Le

---

<sup>1</sup>The cooling time-scales vary roughly as  $n_i^{-1}$ , where  $n_i$  is the density of the ion fluid and is proportional to the H<sub>2</sub> density of the gas - see e.g. Chièze et al. 1998; Lesaffre et al. 2004).

Bourlot et al. 2002). However, we note that, although most of the shocks along the L1157-mm outflow are non-dissociative (or C-type; see Nisini et al. 2010), we cannot rule out the possibility that a compact J-type shock component is present in clump B1, as suggested by the detection of [SiII], [FeII] or [SI] emission arising from this condensation (Neufeld et al. 2009). The final density and initial velocity also determine the maximum temperature attainable by the neutral gas within the shock (Draine et al. 1983 - see Figures 8b and 9b for the assumed values of  $T_{n,max}$  shown in Table 1; Jiménez-Serra et al. 2008). Flower & Pineau des Forêts (2003) predict higher temperatures for the same density and initial velocities at the beginning of the shock than Jiménez-Serra et al. (2008), although the values converge in the middle of the dissipation region. Since, however, recent MHD calculations from van Loo et al. (2009) seem to agree with the lower estimates, we adopt the calculations from Jiménez-Serra et al. (2008); ii) the initial elemental sulfur abundance: we use 1, 1/10 and 1/100 of the solar value; (iii) the degree of depletion, from 1 to 60% of gas depleted by the end of Phase I, an arbitrary range; (iv) the shock velocity from 35 to 60  $\text{kms}^{-1}$ .

Finally as a first attempt at reproducing the *trends* of the molecular line profiles, we input the fractional abundances, densities and temperatures as a function of distance and velocity produced by the chemical and shock model to the radiative transfer model SMMOL (Rawlings & Yates 2001), along with values for the dust temperature and radiation field intensity. The SMMOL code has accelerated  $\lambda$ -iteration, a numerical scheme that solves the exact radiative transfer problem in multilevel non-local conditions, using an approximate lambda operator to derive ‘pre-conditioned’ statistical-equilibrium equations (e.g. Rybicki and Hummer 1991). We ran SMMOL for o-H<sub>2</sub>O, and NH<sub>3</sub>. The collisional data for water and ammonia were taken from Faure et al. (2007) and Danby al. (1988) respectively. New collisional data for ammonia are available (Maret et al. 2009); however as they only cover up to temperatures of 100K and para-H<sub>2</sub>, we have, for this work, used the older data. While

Table 1: Model parameters: Model number, pre-shock density, shock velocity, saturation time, maximum temperature of the neutral gas, degree of depletion at the end of Phase I, and initial sulfur abundance (where 1 stands for solar).

Model	$n(\text{H}_2)$	$V_s$	$T_{sat}$	$T_{n,max}$	Depl.	S
	$\text{cm}^{-3}$	$\text{km s}^{-1}$	yrs	K		
1	$10^5$	40	4.6	4000	1%	1
2	$10^5$	40	4.6	4000	15%	1
3	$10^5$	40	4.6	4000	30%	1
4	$10^5$	35	4.6	3200	30%	1
5	$10^5$	35	4.6	3200	1%	1
6	$10^3$	40	455	2200	10%	1
7	$10^4$	40	45.5	2200	15%	1
8	$10^4$	60	38	4000	30%	1
9	$10^3$	60	380	4000	30%	1
10	$10^3$	60	380	4000	10%	1
11	$10^5$	40	4.6	4000	30%	1/10
12	$10^5$	40	4.6	4000	30%	1/100
13	$10^5$	40	4.6	4000	60%	1
14	$10^4$	40	45.5	2200	60%	1
15	$10^5$	35	4.6	3200	60%	1



water had been modelled by SMMOL before (Lerate et al. 2010) this is the first time that SMMOL was used to model the line intensities and profiles of ammonia. This is the first attempt at using a non LTE non LVG radiative transfer code to model the high resolution H<sub>2</sub>O and NH<sub>3</sub> lines observed by HIFI.

### 3. Results

The aim of this work is to understand qualitatively the origin and history of the molecular gas. Codella et al. (2010) find that the NH<sub>3</sub>/H<sub>2</sub>O intensity ratio decreases at high velocities implying a similar decrease in the abundance ratios. This is the first statement that we will test: Figure 1 shows the chemical evolution of selected species as a function of distance within the shock ( $z$  in units of cm) for four of our models (Model 1, 3, 4 and 7), chosen as examples of variations in depletion, pre-shock densities and shock velocities. We note that the value for the initial abundance of sulfur does not affect the water and ammonia behaviour at all and we won't discuss it further. An increase in depletion efficiency has the effect of increasing all the species that are formed or enhanced on the dust surfaces, but does not affect the abundance trends. Varying the pre-shock density and the shock velocity (and hence the neutral gas shock temperature) has a profound effect on the abundances trends. For Models 1 and 3 water behaves differently from the other three species in that it always remains abundant after the gas cools down, i.e it remains abundant at higher velocities within the post-shock gas ( $v_n > 15 \text{ km s}^{-1}$ ). At first glance, this is certainly consistent with the assumption proposed by Codella et al. (2010) that the NH<sub>3</sub>/H<sub>2</sub>O decrease in intensity at high velocities corresponds to a decrease in their abundance ratio. In Models 4 and 7, on the other hand, ammonia remains high in abundance at high velocities. The key difference among these models is the maximum temperature reached by the gas due to the passage of the shock, and this, in turn, constrains the minimum pre-shock density for the clump (for

models with the same shock velocities). Indeed, if  $v_s = 40 \text{ km s}^{-1}$  only models with initial  $\text{H}_2$  densities greater or equal to  $10^5 \text{ cm}^{-3}$  show temperatures of the neutral fluid of  $\sim 4000 \text{ K}$  in the postshock gas, reproducing the observed differences in the  $\text{NH}_3/\text{H}_2\text{O}$  abundance ratio. The fact that Model 7, where the initial density of the B1 clump is only  $10^4 \text{ cm}^{-3}$ , does not fit the observed behaviour is consistent with previous models of chemically rich clumps along outflows (Viti et al. 2004b), and supports the idea of an inhomogeneous medium with dense pre-existing clumps along L1157. Finally we also note that the observed decrease in the  $\text{H}_2\text{CO}/\text{H}_2\text{O}$  and  $\text{CH}_3\text{OH}/\text{H}_2\text{O}$  abundance ratios with increasing velocity within the shock (Codella et al. 2010), is better reproduced by Models 1 and 3 than by Models 4 and 7.

For ammonia to be abundant in the gas phase alone, high temperatures are required; by running several UCL\_CHEM Phase I test models (with constant densities of  $10^5 \text{ cm}^{-3}$ , with and without freeze out) we find that high abundances (at least  $10^{-6}$ ) of pure gas phase ammonia are only reached if: (i) the temperature is higher than  $800 \text{ K}$  (as its main route of formation,  $\text{H}_2 + \text{NH}_2$ , is endothermic, with a barrier of  $\sim 1400\text{K}$ ); (ii) no substantial freeze out occurs; (iii) the density of the gas is high (in our case  $10^5 \text{ cm}^{-3}$ ) for at least  $10^4$  years. These results are of course consistent with previous findings (see review by Ho & Townes 1983). Taking as an example Model 3, the implications for our L1157 model are as follows: during Phase I of our model, when the temperature is  $10\text{K}$ , the bulk of the ammonia is formed on the grains. During Phase II, the bulk of the ammonia is released from the grain mantles due to sputtering at  $t_{sat} \sim 5$  years (i.e at  $z \sim 5 \times 10^{14} \text{ cm}$ ); however an increase in abundance (from  $4$  to  $6 \times 10^{-5}$ ) does occur during the passage of the shock. The increase corresponds to when the temperature reaches  $\sim 1200\text{K}$  (corresponding to  $v_n \sim 15 \text{ kms}^{-1}$ ), but it is short-lived as  $\text{NH}_3$  starts declining when the temperature reaches  $3500\text{K}$  (corresponding to  $v_n \sim 25 \text{ kms}^{-1}$ ). In terms of emission size of the clump this corresponds to less than  $0.001 \text{ pc}$  ( $0.5''$ – $0.8''$  assuming a distance of  $400$  and  $250 \text{ pc}$  respectively). This

implies that observations of  $\text{NH}_3$  toward the B1 clump with single dishes ( $\sim 20''$ – $40''$ ) would then give lower  $\text{NH}_3$  abundances than those predicted by our model due to beam dilution (i.e.  $5 \times 10^{-5} \times [1'' / (20'' - 40'')]^2 \sim 10^{-7} - 3 \times 10^{-8}$ ). We note that these diluted abundances are similar to those reported by Bachiller et al. (1993) toward the B1 clump. High-angular resolution observations of high-excitation lines of  $\text{NH}_3$  with the VLA are therefore required to establish the length of the region within the postshock gas where  $\text{NH}_3$  is expected to be enhanced.

The degree and extent of the increase in the  $\text{NH}_3$  abundance due to gas phase high temperature chemistry will also depend on the degree of depletion adopted in Phase I; for example, if one compares Model 1 and Model 3 (where 1% and 30% of the gas phase is depleted by the end of Phase I, respectively) one notes that in Model 1 the relative increase is more substantial (at  $\sim 3 \times 10^{15}$  cm), due to the lower  $\text{NH}_3$  abundance released from the grains in Phase II.

Ultimately, therefore, the difference between the water and ammonia behaviours between Models 1 and 3, and Models 4 and 7 is due to the temperature: in a model where the initial density is  $< 10^5 \text{ cm}^{-3}$ , or the velocity is  $< 40 \text{ kms}^{-1}$ , the maximum temperature reached by the C-shock is  $\sim 3000 \text{ K}$ . Under these conditions ammonia is maintained high as there is no effective destruction route while it can efficiently form via the reaction  $\text{H}_2 + \text{NH}_2$ . For models where the temperature during the shock is  $\sim 4000 \text{ K}$ , ammonia is instead efficiently destroyed by the reaction:  $\text{H} + \text{NH}_3 \Rightarrow \text{NH}_2 + \text{H}_2$ . The latter has a high barrier ( $\sim 5000 \text{ K}$ ) and hence it is inefficient for models where the maximum temperature of the shock is lower than  $4000 \text{ K}$ . The main reaction that forms water, on the other hand, is very efficient as long as temperatures are over  $220 \text{ K}$  while the main destruction route (via reaction with atomic hydrogen) has a very high barrier ( $\sim 9000 \text{ K}$ ).

As the discriminating factor seems to be the maximum temperature attained by

the shock we note that if the shock velocity is higher (e.g.  $60 \text{ km s}^{-1}$ ) then low initial densities may still lead to maximum temperatures of  $\sim 4000\text{K}$  (Models 8-10). However we find that, regardless of the shock parameters, low initial densities imply that the gas abundances of water and ammonia (and other species) do not reach high values until the shock is at least half way through the dissipation region, leading to underestimated column densities. Moreover, if a shock velocity of  $60 \text{ km s}^{-1}$  were present toward B1, we should expect to detect  $\text{H}_2\text{O}$  at much higher terminal velocities than observed ( $\sim 30 \text{ km s}^{-1}$ ). These qualitative comparisons indicate that the best fit dynamical model for L1157 is one where the shock velocity is  $\sim 40 \text{ km s}^{-1}$  and  $n_H \sim 10^5 \text{ cm}^{-3}$ .

Comparing our water abundances with those found by Lefloch et al. (2010) we are in good qualitative agreement: they find that the water is enhanced by two orders of magnitude between the low (from  $V_{LSR}=2.5$  to  $-6 \text{ km s}^{-1}$ ) and high-velocity (from  $V_{LSR}=-6$  to  $-25 \text{ km s}^{-1}$ ) components from  $8 \times 10^{-7}$  to  $8 \times 10^{-5}$  respectively; comparing these abundances with our lowest pre-shock water abundances of  $8 \times 10^{-7}$  (corresponding to  $V_{LSR}$  up to  $-6 \text{ km s}^{-1}$ ) and the high abundance reached during the shock of  $\sim 2 \times 10^{-4}$  (from  $-7$  to  $-30 \text{ km s}^{-1}$ ), respectively; the latter is a factor of 3 higher than observed; we consider a match within a factor of three as a good agreement.

Finally, we test whether the profile of the water line does indeed differ from that of ammonia. We have used the velocity, abundance, temperature and density profiles from Models 3 and 4 as input to our radiative transfer model SMMOL and we computed the line profiles for water and ammonia. Figure 2 shows water and ammonia profiles for Model 3, overplotted with the ammonia profile for Model 4 (the water profile for Model 4 is very similar to that of Model 3). Clearly, while certainly not a match, the line profile for water is different from that of ammonia for Model 3, and in particular it extends to higher velocities. Moreover, in very good agreement with the observations, the water intensity is about a

factor of 7 higher than that of ammonia (the latter is multiplied by this factor in the figure - see caption). On the contrary, the  $\text{NH}_3$  profile for Model 4 extends at higher velocities and its intensity is higher than observed (in the figure it is multiplied by a factor of 5). This is the first time that modelling very high resolution profiles of water and ammonia in shocked regions starting from a pure ab initio approach has been attempted. Note that we do not aim at a quantitative match with the high resolution HIFI spectra: this would require a better knowledge of the geometry and structure of the B1 clump and most importantly a three dimensional radiative transfer model. Nevertheless this first attempt is very promising as we are in fact able to reproduce how the  $\text{NH}_3/\text{H}_2\text{O}$  intensity ratio changes with velocity.

### Acknowledgements

IJS acknowledges the Smithsonian Astrophysical Observatory for the support provided through a SMA fellowship.

### References

- Bachiller R., R.; Martínn-Pintado, J.; Fuente, A., 1993, ApJ, 417, L45
- Bachiller R., & Pérez Gutiérrez M. 1997, ApJ, 487, L93
- Bachiller R., Pérez Gutiérrez M., Kumar M.S.N., & Tafalla M. 2001, A&A 372, 899
- Benedettini, M, Yates, J A, Viti S, Codella C, 2006, MNRAS, 370, 229
- Benedettini M., Viti, S.; Codella, C.; Bachiller, R.; Gueth, F.; Beltrán, M. T.; Dutrey, A.; Guilloteau, S., 2007, MNRAS, 381, 1127
- Beuther H., Thorwirth, S., Zhang, Q., Hunter, T. R., Megeath, S. T., Walsh, A. J., Menten, K.

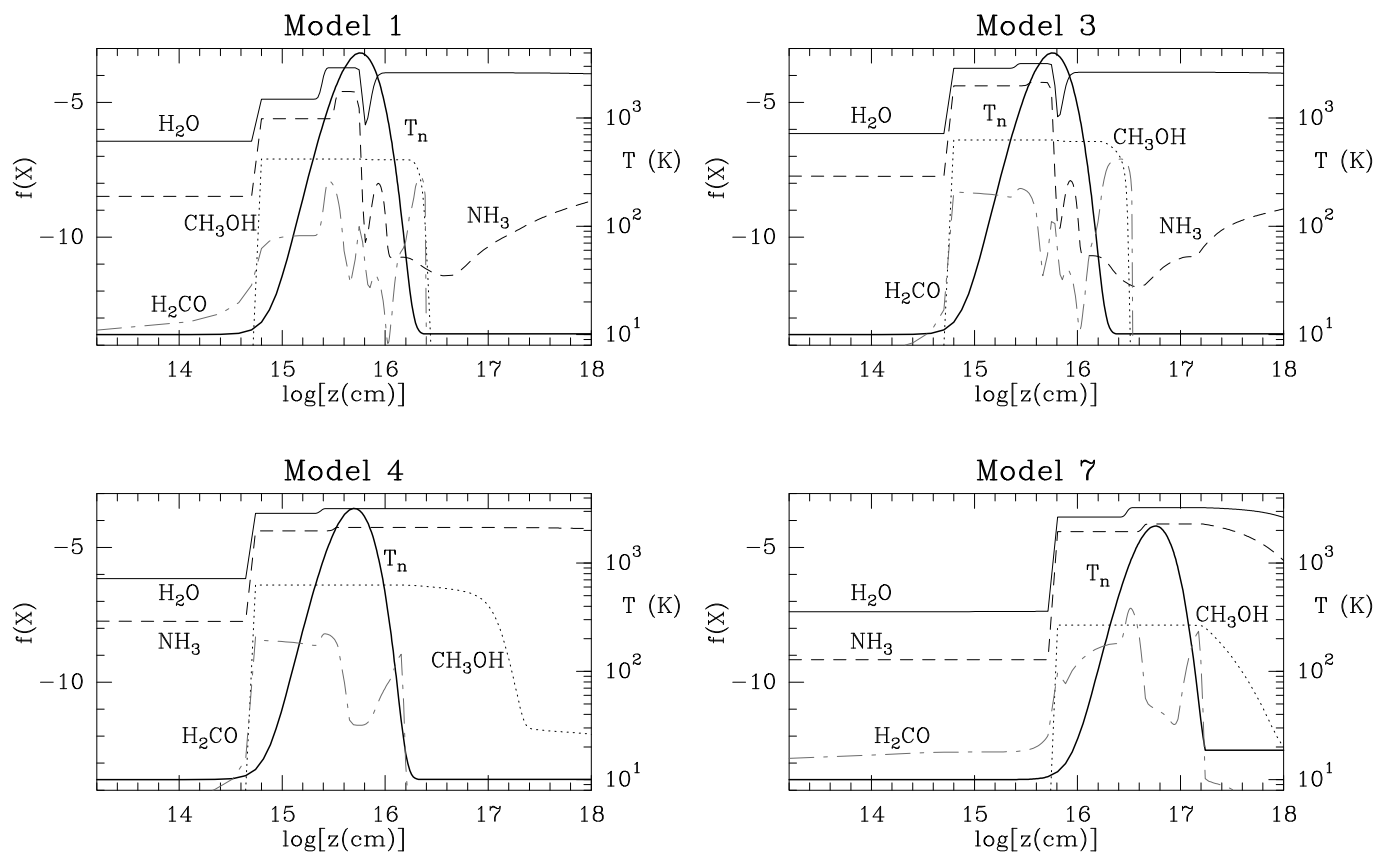


Fig. 1.— Fractional abundances (with respect to molecular hydrogen), of selected species as a function of distance for Phase II for Models 1, 3, 4 and 7. The temperature profile for each model is also shown.

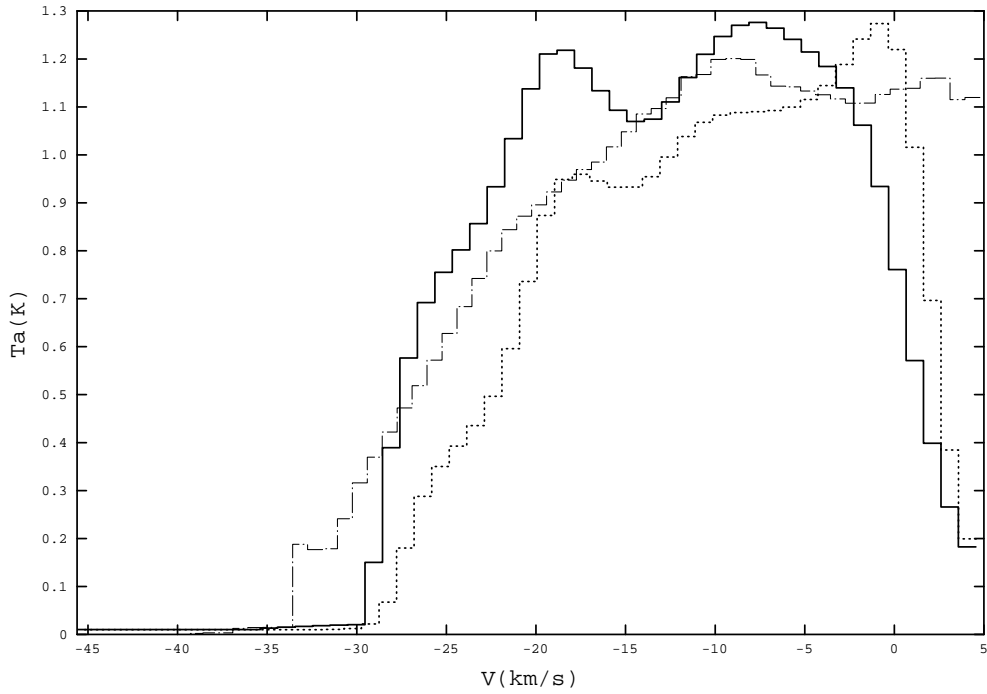


Fig. 2.— Theoretical line profiles of  $\text{H}_2\text{O}(1_{10}-1_{01})$  (solid line), and  $\text{NH}_3(1_0-0_0)$  (dotted line) for Model 3. The profile of the  $\text{NH}_3$  line has been multiplied by a factor of 7.5. The  $V_{LSR}$  is  $+2.6 \text{ km s}^{-1}$ . We also overplot the theoretical line profile of  $\text{NH}_3(1_0-0_0)$  (dot-dash line) for Model 4, multiplied by a factor of 5.

- M., 2005, *ApJ*, 627, 834
- Brown P. D., Charnley, S. B., Millar, T. J., 1988, *MNRAS*, 231, 409
- Caselli, P., Hartquist, T. W., & Havnes, O. 1997, *A&A*, 322, 296
- Ceccarelli C., Bacmann A., Boogert A., et al., 2010, *A&A*, 521, L22
- Chieze, J.-P.; Pineau des Forêts, G.; Flower, D. R., 1998, *MNRAS*, 295, 672
- Codella C., Benedettini M., Beltrán M.T., et al. 2009, *A&A*, 507, L25
- Codella C., Lefloch B., Ceccarelli, C., et al. 2010, *A&A*, 518, L112
- Danby G., Flower D. R., Valiron P. Shilke P., 1988, *MNRAS* 235, 229
- Draine B. T.; Roberge, W. G.; Dalgarno, A., 1983, *ApJ*, 264, 485
- Faure A, Crimier N, Ceccarelli C, Valiron P, Wiesenfeld L, Dubernet M L, 2007, *A&A*, 472, 1029
- Flower, D. R., & Pineau des Forêts, G. 2003, *MNRAS*, 343, 390
- Gueth F., Guilloteau S., & Bachiller R. 1996, *A&A* 307, 891
- Ho P T P, Townes C H, 1983, *ARA&A*, 21, 239
- Jiménez-Serra, I., Caselli, P., Martín-Pintado, J., & Hartquist, T. W. 2008, *A&A*, 482, 549
- Jiménez-Serra, I.; Martín-Pintado, J., Rodríguez-Franco, A., & Martín, S. 2005, *ApJ*, 627, L121
- Kaufman, M. J., & Neufeld, D. A. 1996, *ApJ*, 456, 250
- Garay G., Köhnenkamp I., Bourke T.L., Rodríguez L.F., & Lehtinen K.K. 1998, *ApJ*, 509, 768
- Gusdorf A., Pineau Des Forêts G., Cabrit S., & Flower D.R. 2008, *A&A* 490, 695
- Jørgensen J.K., Bourke T.L., & Myers P.C. 2007, *ApJ*, 659, 479
- Le Bourlot, J.; Pineau des Forts, G.; Flower, D. R.; Cabrit, S., 2002, *MNRAS*, 332, 985
- Lefloch B., Cabrit S., Codella C., et al. 2010, *A&A*, 518, L113
- Lerate, M. R.; Yates, J. A.; Barlow, M. J.; Viti, S.; Swinyard, B. M., 2010, *MNRAS*, 406, 2445
- Lesaffre P.; Chiéze, J.-P.; Cabrit, S.; Pineau des Forêts, G, 2004, *A&A*, 427, 147L
- Maret, S.; Faure, A.; Scifoni, E.; Wiesenfeld, L., 2009, *MNRAS*, 399, 425
- May, P. W., Pineau des Forêts, G., Flower, D. R., Field, D., Allan, N. L., & Purton, J. A. 2000, *MNRAS*, 318, 809



Neufeld D A; Nisini, B; Giannini, T; Melnick, G J.; Bergin, E A; Yuan, Y; Maret, S.; Tolls, R.; Güsten,lf; Kaufman, M J., 2009, ApJ, 706, 170

Nisini, B, Giannini, T, Neufeld, D, Yuan, Y, Antonucci, S, Bergin, E A, Melnick, G, 2010, ApJ, 724, 69

Rawlings J. M. C.; Yates, J. A., 2001, MNRAS, 326, 1423

Rawlings J. M. C.; Hartquist, T. W.; Menten, K. M.; Williams, D. A., 1992, MNRAS, 255, 471

Rybicki G. B., Hummer D. G., 1991, A&A, 245, 171

Sepulveda I., Anglada, G., Estalella, R., López, R.; Girart, J. M., Yang, J., 2011, A&A, 527, 41

Tafalla M., & Bachiller R. 1995, ApJ 443, L37

van Loo, S.; Ashmore, I.; Caselli, P.; Falle, S. A. E. G.; Hartquist, T. W., 2009, MNRAS, 395, 319

Viti, S, Collings, M P, Dever, J W, McCoustra M R S, Williams D A, 2004, MNRAS, 354, 1141

Viti, S, Codella, C, Benedettini M, Bachiller R, 2004, MNRAS, 350, 1029

Zhang Q., Ho T. P., Wright M. C. H., Wilner D. J., 1995, ApJ, 451, L71